Pressure effects for crystal growth in a closed system

Massimo Conti
Dipartimento di Fisica, Universitá di Camerino, and Istituto Nazionale di Fisica della Materia, Via Madonna delle Carceri, I-62032, Camerino, Italy

(Received 22 January 2004; revised manuscript received 7 June 2004; published 10 September 2004)

We analyze the growth of a crystal from its supercooled liquid in a *closed* domain (constrained growth), taking into account the effects due to the different densities ρ_s and ρ_l of the solid and liquid phases. We assume $\rho_l > \rho_s$, i.e., the liquid expands upon solidification. Then, the growth is contrasted by an increasing pressure, which results in a continuous decrease of the coexistence temperature and the effective supercooling. These phenomena have been simulated in two dimensions through a modified version of the classic phase-field model. We observe that for spherical growth the interface temperature reflects almost instantaneously the change of the coexistence temperature. For dendritic growth, we observed a relaxation time for the dendrite tip velocity and the tip radius which is comparable to the characteristic time of the process; however, after the first fast transient, the growth dynamics seems to follow the changing pressure with no appreciable lag. The onset of the morphological instability is slightly anticipated in respect to free growth.

DOI: 10.1103/PhysRevE.70.031602 PACS number(s): 81.10.Mx, 05.70.Fh, 64.70.Dv, 05.70.Ln

I. INTRODUCTION

Solidification from a supercooled melt is generally addressed as a diffusion controlled process, as the latent heat released at the solid-liquid interface must be rejected away from the advancing front [1]. In this sense, the only external parameter available to control the process is the supercooling imposed at infinity $\Delta = C(T_0 - T_\infty)/L_0$, where C is the specific heat, T_0 represents the coexistence temperature of the solid and liquid phases and L_0 the latent heat per unit mass. This picture is valid, to a first approximation, in absence of buoyancy effects (i.e., in a microgravity environment) [2]. However, even in this case, the volume change in solidification is the source of a richer phenomenology, which deserves further investigation. In this perspective, some experimental investigations stressed the role of pressure as a possible control variable in solidification experiments. The melting temperature changes with pressure according to the Clapeyron equation; then pressure variations during solidification allow the researcher to control in a rapid and uniform way the actual supercooling of the melt [3,4]. It has also been shown that the frequency of dendritic side-branching can be tuned by periodic pressure variations, to induce a regularization of the growth pattern [5,6].

The Clapeyron's effect can play also a role for solidification in a closed system, i.e., at constant volume. When $\rho_l < \rho_s$ (contraction) tensile stresses eventually result in the formation of cavities, where the pressure level is fixed by the local vapor pressure; when $\rho_l > \rho_s$ the liquid expands upon solidification, and the pressure increases with time due to the mechanical constraint of the domain's walls. The latter case, typical for water, is of central relevance in geological processes. Moreover, recent experiments on the melting and solidification of nanoscale crystals, encapsulated in fullerene-like graphitic shells, put into evidence significant alterations of the phase-change dynamics; the overpressure due to the carbon shell seems to be responsible of some of these effects [7].

In this paper we address the growth of a crystal in a *closed* system, using a modified version of the phase-field model [8], which takes into account the hydrodynamic and elastic corrections to the classic diffusive problem. The model is a refinement of a previous approach [9], with a more consistent derivation of the thermodynamic potential, and incorporates also ideas proposed by Caginalp and Jones [10], Oxtoby [11], Anderson *et al.* [12], and Tong *et al.* [13]. We assume $\rho_l > \rho_s$, i.e., the liquid expands upon solidification. The aim of our investigation is to characterize the interplay between the (fast) relaxation of the mechanical modes and the (slow) relaxation of the thermal field. The model has been solved numerically in two dimensions to describe the spherical growth of a solid nucleus, with isotropic and anisotropic surface tension. In the first case we observe that during the growth, the interface temperature can be well approximated through the Clapeyron's equation, with the usual capillary and kinetic corrections. This indicates that even in presence of strong elastic transients, the interface kinetics is essentially driven by the average pressure inside the system. Along the growth, due to the morphological instability, the crystal loses its spherical shape [14]. We observed that in respect to nonconstrained growth, the onset of this instability is slightly anticipated. With anisotropic surface tension, the solid seed develops into the well known *needle crystal* (or free dendrite). As shown by Ivantsov [15], the purely diffusive solution is a shape-preserving parabola which moves at constant velocity. The Peclet number, i.e., the product of the tip radius R_{tip} and the tip velocity v_{tip}, is uniquely fixed by the supercooling Δ. Our numerical simulations show that in a closed system the increasing pressure alters significantly the growth dynamics, destroying the steady regime; to follow the decreasing supercooling, the Peclet number changes with time. We observed that the relaxation time for this phenomenon is comparable to the characteristic time of the process; however, after the first fast transient, the growth dynamics seems to follow the changing pressure with no appreciable lag.

II. THE EQUATIONS OF THE MODEL

The governing equations of the model are derived in full details in Ref. [8]. The order parameter ϕ takes the values $\phi=0$ in the solid and $\phi=1$ in the liquid. The solid phase is modelled as an isotropic fluid with large viscosity. We indicate with T_0, p_0, ρ_{s0}, ρ_{l0} the temperature, pressure, solid, and liquid density, respectively, in an equilibrium reference state. The equilibrium density $\rho_0(\phi)$ is assumed to change in the interfacial region as $\rho_0 \equiv \rho_0(\phi)=\rho_{s0}+p(\phi)(\rho_{l0}-\rho_{s0})$, where the function $p(\phi)=\phi^3(10-15\phi+6\phi^2)$ is monotonic and increasing with ϕ, taking the values $p(0)=0$, $p(1)=1$. A nondimensional form of the model equations is obtained adopting a reference length ξ and scaling time to $\tau=\xi^2/D$ (D is the thermal diffusivity). Density is scaled as ρ/ρ_{l0} and a nondimensional temperature is introduced as $u=C(T-T_0)/L_0$. Specific energies will be scaled to v_0^2, where $v_0=\xi/\tau$, and the scale for pressure and the components of the stress tensor is $\rho_{l0}v_0^2$. Notice that in the following we neglect thermal expansion effects; moreover equal values in both phases are assumed for the specific heat, the thermal diffusivity and the isothermal compressibility.

Then, the model equations read

$$\frac{d\rho}{dt} = -\rho\vec{\nabla}\cdot\vec{v}, \tag{1}$$

$$\rho\frac{d\vec{v}}{dt} = \vec{\nabla}\cdot(\mathbf{T}+\mathbf{\Pi}), \tag{2}$$

$$\frac{du}{dt} + p'(\phi)\frac{d\phi}{dt} = \nabla^2 u + \frac{1}{\rho R_5}(\mathbf{\Pi}:\vec{\nabla}\vec{v}), \tag{3}$$

$$\frac{d\phi}{dt} = m\left\{\vec{\nabla}\cdot(\eta^2(\theta)\vec{\nabla}\phi) + \frac{\partial}{\partial y}[\eta(\theta)\eta'(\theta)\phi_x] - \frac{\partial}{\partial x}[\eta(\theta)\eta'(\theta)\phi_y]\right\} - \frac{m}{\tilde{\epsilon}^2}\left[\frac{\partial g(\phi)}{\partial\phi} - p'(\phi)\rho\alpha\tilde{\epsilon}u\right] - \frac{1}{2}p'(\phi)\rho(1-S)R_1\left(\frac{\rho_0^2-\rho^2}{\rho^2\rho_0^2}\right), \tag{4}$$

where $\mathbf{T}$ and $\mathbf{\Pi}$ indicate, respectively, the capillary and the viscous stress tensor, which components are

$$T_{xx} = -p_0 - \frac{R_1R_3}{m}\frac{(\rho-\rho_0)}{\rho} + R_2\rho_y^2 + R_3\phi_y^2,$$

$$T_{yy} = -p_0 - \frac{R_1R_3}{m}\frac{(\rho-\rho_0)}{\rho} + R_2\rho_x^2 + R_3\phi_x^2,$$

$$T_{xy} = T_{yx} = -R_2\rho_x\rho_y - R_3\phi_x\phi_y,$$

$$\Pi_{xx} = R_4\lambda(\phi)\left(\frac{4}{3}\frac{\partial v_x}{\partial x} - \frac{2}{3}\frac{\partial v_y}{\partial y}\right) + R_7\vec{\nabla}\cdot\vec{v},$$

$$\Pi_{yy} = R_4\lambda(\phi)\left(\frac{4}{3}\frac{\partial v_y}{\partial y} - \frac{2}{3}\frac{\partial v_x}{\partial x}\right) + R_7\vec{\nabla}\cdot\vec{v},$$

TABLE I. Material properties utilized to evaluate the model parameters.

Parameter	Value	
ρ_{l0}	8.040×10^3	Kg m^{-3}
L_0	2.93×10^5	J Kg^{-1}
T_0	1.728×10^3	K
C	4.44×10^2	J Kg^{-1} K^{-1}
D	1.54×10^{-5}	m^2 s^{-1}
γ	0.8	J m^{-2}
μ	2.62	m s^{-1}K^{-1}
k	5.56×10^{-12}	m^3 J^{-1}
$\eta_l=\zeta_l$	1.30×10^{-3}	J s m^{-3}

$$\Pi_{xy} = \Pi_{yx} = R_4\lambda(\phi)\left(\frac{\partial v_x}{\partial y} + \frac{\partial v_y}{\partial x}\right). \tag{5}$$

In the above equations the parameters are defined as

$$m = \frac{\mu\gamma T_0}{D\rho_{l0}L}, \quad \tilde{\epsilon} = \frac{h}{\xi}, \quad \alpha = \frac{\xi}{6\sqrt{2}d_0},$$

$$R_1 = \frac{\mu\tau T_0}{6\sqrt{2}hk\rho_{l0}L}, \quad R_2 = R_3 = \frac{6\sqrt{2}\gamma h}{\xi^2\rho_{l0}v_0^2},$$

$$R_4 = \frac{\eta_l}{\tau\rho_{l0}v_0^2}, \quad R_5 = \frac{L_0}{v_0^2}, \quad R_7 = \frac{\zeta_l}{\tau\rho_{l0}v_0^2}, \tag{6}$$

where γ is the surface tension, h is the interface thickness, and $d_0=(\gamma CT_0)/(\rho_0L_0^2)$ is the capillary length. Moreover, μ is the kinetic supercooling coefficient that relates the interface supercooling to the interface velocity v_I through $v_I=\mu(T_0-T)$; k is the isothermal compressibility and η_l, ζ_l represent the first and second viscosity in the liquid. The function $g(\phi)=(1/4)\phi^2(1-\phi)^2$ is the classic double-well Landau-Ginzburg contribution to the free energy. Anisotropy of the surface energy is accounted for through the function $\eta(\theta)=(1+\omega\cos 4\theta)$, where θ is defined as the angle between the normal to the interface and a fixed direction, the x axis in our calculations, and ω specifies the intensity of the anisotropy. The function $\lambda(\phi)$ describes the transition of the system's viscosity across the interface. In the bulk solid we assumed $\eta_s=10^3\eta_l$. To allow a complete relaxation of the order parameter towards the stable solid phase in a reasonable time, we defined $\lambda(\phi)=\eta_s/\eta_l+q(\phi)(1-\eta_s/\eta_l)$ with $q(\phi)=1$ for $\phi\geqslant 0$ and $q(\phi)=0$ for $\phi=0$. Table I summarizes the values of the thermophysical properties we used to estimate the model parameters; notice that we referred to the phase diagram and to the elastic properties of nickel. The interface thickness has been chosen as $h=30\times10^{-8}$ cm. Choosing an (arbitrary) length scale $\xi=2\times10^{-4}$ cm, we have the following values of the parameters: $\alpha=265$, $m=0.1$, $\tilde{\epsilon}=1.5\times10^{-3}$, $R_1=3.53\times10^6$, $R_2=R_3=1.07\times10^{-2}$, $R_4=R_7=0.105$, $R_5=4.94\times10^3$. The density ratio is chosen as $S=0.85$.

III. NUMERICAL RESULTS

Equations(1)–(4) have been solved on a computational domain $0 \leqslant x \leqslant x_m$, $0 \leqslant y \leqslant y_m$, with impermeable boundary conditions. Time integration was exploited through an explicit scheme except for the momentum equations, in which, due to the large viscosity of the solid phase, we were forced to employ an implicit scheme. Second order central differences were used for the Laplace operator, and upwind differences for the convective terms. The grid spacing was selected as $\Delta x = \Delta y = \tilde{\epsilon}$; the time step required for numerical stability is $\Delta t = 0.36 \times 10^{-6}$. Following a standard method in computational fluid dynamics, the velocity fields v_x, v_y were solved on two computational grids shifted of $\Delta x/2$ and $\Delta y/2$ in respect to the one used for the scalar fields.

A. Spherical growth

Let us first consider the isotropic growth ($\omega = 0$) of a spherical nucleus. We choose $x_m = y_m = 1.8$. Initially, the uniform supercooled melt ($\Delta = 0.7$) is at rest ($\phi = 1, \rho = 1, v_x = 0, v_y = 0, u = -\Delta$); then a circular solid seed ($\phi = 0, \rho = S, u = 0$) is nucleated, with center at $x = x_m/2$, $y = y_m/2$ and a supercritical radius $R_0 = 0.012$. Here and in the following the numerical results will be reported in nondimensional units. For the reader's convenience we recall that the length scale is 2×10^{-4} cm, the velocity scale 7.70×10^2 cm s^{-1} and the time scale 2.58×10^{-7} s. The pressure scale is 4.77×10^5 Pa.

In the first stage of the growth surface tension effects prevail, and the crystal preserves a circular shape; then, after the onset of the morphological instability, the spherical symmetry is destroyed. Figures 1(a)–1(c) show the pressure field in the liquid at three different times. The first picture shows the sharp pressure step around the crystal (the white spot at the center of the graph), due to the sudden expansion of the solidified melt. Then the pressure wave reaches the domain's boundaries, where it is reflected and redirected towards the crystal [Figs.1(b) and 1(c). The sequence of the pictures shows that the average pressure increases with time, as any volume change of the system is prevented by the impermeable walls. Then, as predicted by the Clapeyron's equation, we expect a drop of the effective supercooling along the growth. This effect is evidenced in Fig. 2 where the growth rate is represented versus time. For comparison we show also the data obtained with an identical system, with *permeable* boundary conditions. In a first stage the two curves coincide (until the reflected wave impinges on the crystal's surface). Then the growth rate in free conditions approaches asymptotically a constant value. For constrained growth, on the contrary, we see the continuous slowing of the process, due to the decrease of the thermodynamic force available for solidification.

To better understand the extent of this effect, we observe that the Clapeyron's equation, in nondimensional form, may be written as

$$u_\pi = \frac{\tilde{\epsilon}}{\alpha} \frac{S-1}{S} \frac{1}{R_3} (p - p_0), \tag{7}$$

where u_π, the shift of the coexistence temperature, is related to the pressure shift $(p - p_0)$. The latter, averaged over the entire system, may be estimated as

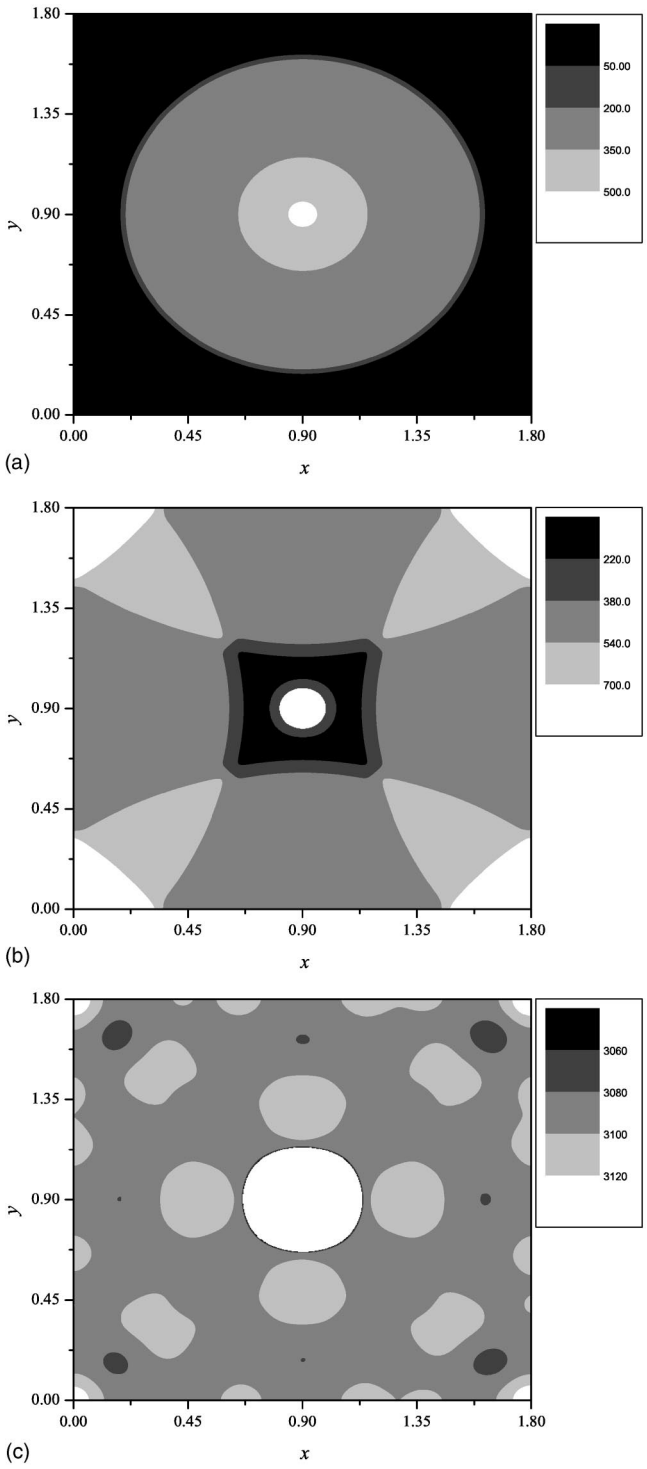

FIG. 1. The pressure wave originated at the solid-liquid interface, at times 1.15×10^{-3} (a), 2.52×10^{-3} (b), and 2.52×10^{-2} (c). Notice the increase with time of the average pressure.

$$\langle p - p_0 \rangle = \frac{R_1 R_3}{m} \left[\frac{1}{1 + x_s(S-1)} - 1 \right], \tag{8}$$

where x_s is the actual solid fraction. We recall also that for a solid-liquid interface with curvature κ, the equilibrium temperature shift, due to the Gibbs-Thomson effect, is

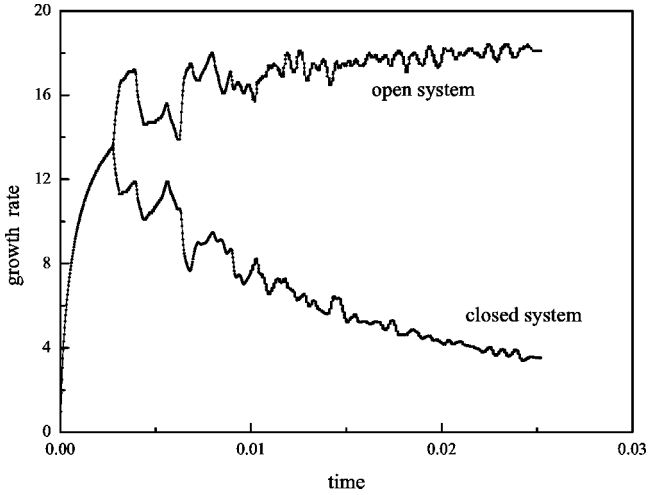

FIG. 2. The growth rate versus time for spherical growth in an open and a closed system.

$$u_\kappa = -\frac{\kappa}{6\sqrt{2}\alpha}. \tag{9}$$

Figure 3 shows, versus time, the interface temperature as obtained through the numerical simulation, compared with the contributions u_π and $u_\pi + u_\kappa$.

We observe that the numerical solution agrees to a quite good extent with the pressure plus curvature shifts obtained using the actual solid fraction and the curvature of the crystal. This means that the interface temperature follows almost instantaneously the change of the actual supercooling.

For the free growth of a spherical nucleus, the linear analysis of Mullins and Sekerka [14] can determine the largest radius $R=R^*$ of the crystal which still corresponds to a stable symmetric growth. An interesting question is whether the onset of the morphological instability is altered in a closed system. To estimate R^* we observe that, due to the finite spacing of the grid, the symmetry of the crystal is very poor in the early stage of the growth, and improves with time

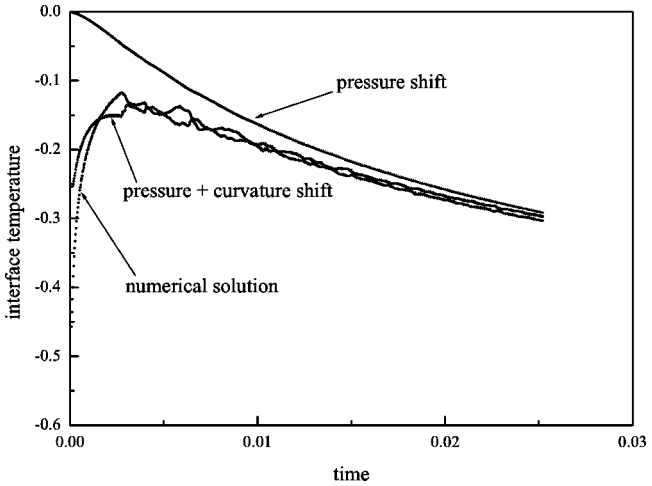

FIG. 3. Interface temperature versus time for spherical growth. The numerical solution is compared with the pressure and curvature corrections to the coexistence temperature.

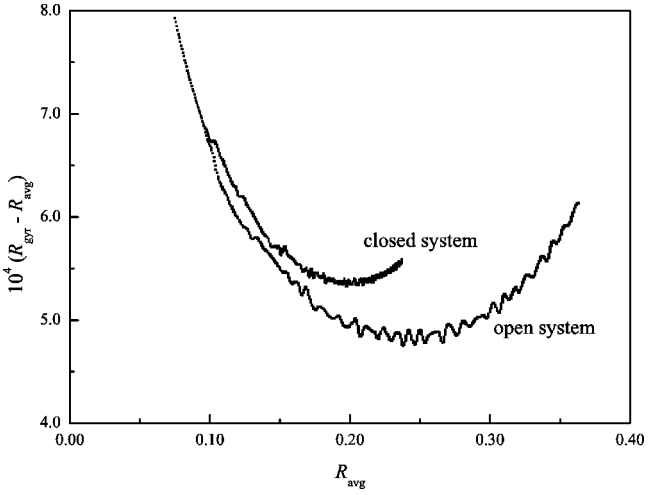

FIG. 4. The difference between the gyration radius of the crystal and the average radius R_{av}, versus R_{av}. The two curves show that for constrained growth the loss of spherical symmetry is slightly anticipated with respect to free growth.

until $R \leqslant R^*$, when the crystal begins to lose its sphericity. A simple indicator for the deviations of the crystal from the circular shape may be constructed considering the first and the second moment of its radius, i.e., the average radius R_{av} and the gyration ratio R_{gyr}. The difference $R_{gyr} - R_{av}$ vanishes for a symmetric disk and increases when the circular symmetry is lost. We estimated the average radius as $R_{av} = \sqrt{A_{sol}/\pi}$, with A_{sol} indicating the total area of the solidified mass. Indeed, Fig. 4 shows that this difference, represented versus R_{av}, first diminishes, traverses a minimum and then, after the onset of the instability, increases with increasing the size of the crystal. The position of the minimum can be assumed as a reasonable estimation of $R=R^*$. We observe in the figure that for constrained growth the onset of the instability is slightly anticipated with respect to free growth. This effect is consistent with the results of a previous investigation [16] which pointed out that the stability of the growth increases with increasing the effective supercooling.

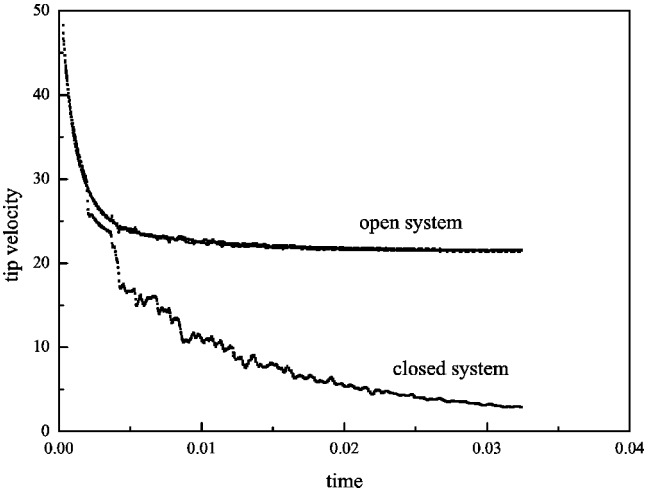

FIG. 5. Dendritic growth. Tip velocity versus time in a open and a closed system.

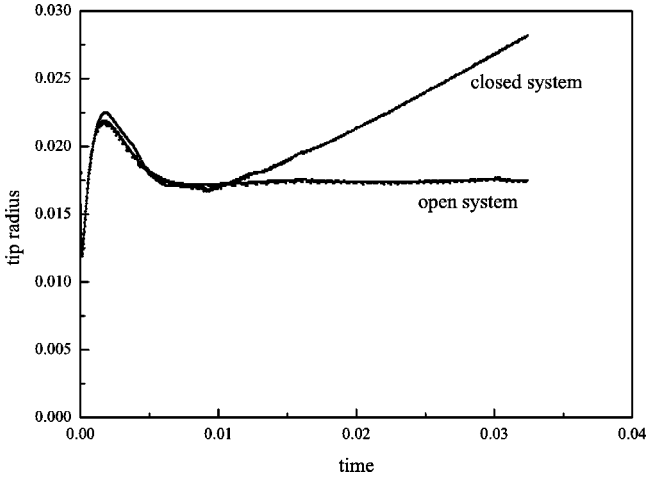

FIG. 6. Dendritic growth. Tip radius versus time in a open and a closed system.

B. The needle crystal

Another set of experiments, with $\omega=0.03$ and $\Delta=0.7$, is concerned with dendritic growth. We set a circular seed centered at $x=0$, $y=y_m/2$, with a supercritical radius $R_0=0.012$. After the onset of the morphological instability, the pattern selected by the system is a needle crystal propagating along the x axis. Figures 5 and 6 show, versus time, the velocity and the radius of the dendrite tip. We observe, for an open system, the well-known steady regime. On the contrary, in a closed system the growth is characterized by a continuous decrease of the effective supercooling $\Delta^*=\Delta+u_\pi$, so that the tip velocity decreases with time and the tip radius increases. According to the Ivantsov's analysis, in *steady* conditions the Peclet number, defined as $P=0.5(R_{\mathrm{tip}}v_{\mathrm{tip}})$, should only depend on the melt supercooling. An interesting question is whether in a closed system the growth follows a quasisteady dynamics, adapting instantaneously to the variation of the effective supercooling Δ^*. In Fig. 7 we show the decrease of the Peclet number along the growth (solid line), reflecting the decrease of the effective supercooling. On the same graph we superimposed (diamonds) some values of the Peclet number obtained for *steady* growth in an open system, with values of the supercooling Δ corresponding to the instantaneous values of Δ^*. We observe that the steady values of the Peclet number represent a good approximation to the dynamic evolution of the process except for the first fast transient (notice that we were not able to obtain steady solutions with $\Delta\leqslant 0.55$).

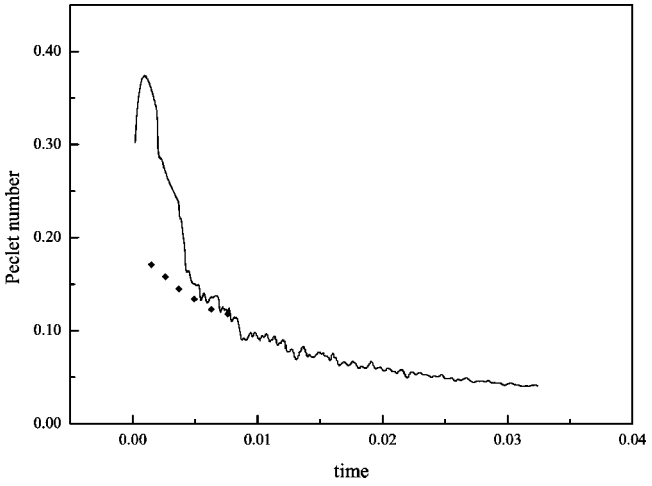

FIG. 7. Dendritic growth. The Peclet number versus time (solid line). The diamonds represent the Peclet number obtained for steady growth in a open system, with values of the supercooling Δ corresponding to the instantaneous values of the actual supercooling Δ^*. From left to right these correspond to $\Delta=0.675, 0.650, 0.625, 0.600, 0.575, 0.550$.

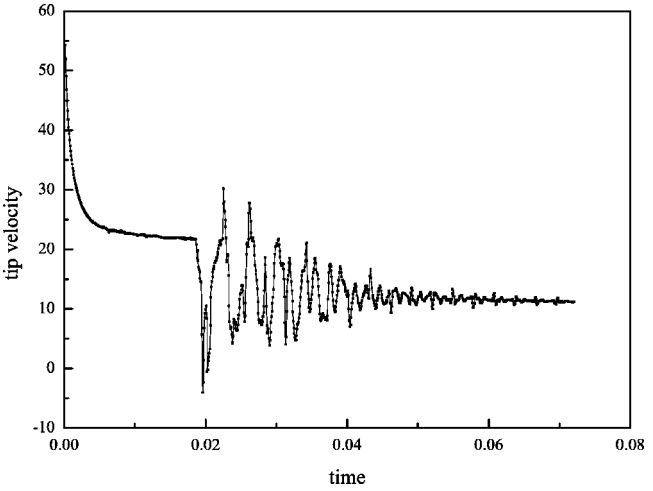

FIG. 8. Dendritic growth. Tip velocity versus time before and after the step variation of the external pressure, which occurs at time $t=0.02$.

To get some insight into this issue, we planned a different experiment. During the free growth of a needle crystal, after the steady regime was achieved, we impressed a step variation of the external pressure (from $p=0$ to $p=1200$). The transition of the system towards the new regime is shown in Figs. 8 and 9, where the tip velocity and the tip radius are

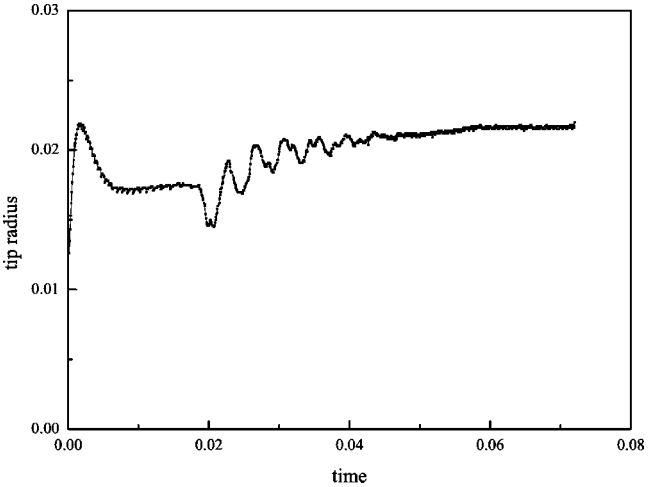

FIG. 9. Dendritic growth. Tip radius versus time before and after the step variation of the external pressure, which occurs at time $t=0.02$.

represented versus time. We observe that the transition is not instantaneous, and takes a time of the order of $\Delta t \sim 0.02$. This lag, at least in our case (solidification far from equilibrium), is not irrelevant with respect to the time scale of the growth process, and in a fast transient we are not allowed to decouple the growth dynamics from the pressure change. It is worth to notice that the time scale we observed for the relaxation of the system is in qualitative agreement with the numerical and experimental results obtained by Börzsönyi [5,6] in the *frequency* domain. These authors studied the dynamic response of dendritic solidification to periodic pressure variations, focussing their attention on the emission of side branches. A resonance behavior was detected at frequencies of the order of $f \sim 100$; at frequencies larger than these, the growth could not follow the external forcing.

IV. CONCLUSIONS

The results of this investigation show that volumetric effects can influence constrained crystal growth in a significant manner. The melting temperature shift driven by the pressure change along the growth reduces the thermodynamic force available for solidification. The interface temperature changes with time, and may be evaluated with a good accuracy through the Clapeyron equation and the curvature correction. The onset of the morphological instability, for a spherical crystal, is slightly anticipated with respect to free growth. In dendritic solidification the melting temperature shift destroys the steady regime, and the tip radius and velocity change with time. We observed that the relaxation time for this phenomenon is comparable to the characteristic time of the process, and consistent with the results of previous investigations conducted in the frequency domain. However, after the first fast transient, the Peclet number seems to be well approximated by the values obtained in steady conditions, with a supercooling corresponding to the instantaneous actual supercooling. This indicates that a quasisteady approximation is a satisfactory approach to interpret the growth dynamics.

[1] J. S. Langer, Rev. Mod. Phys. **52**, 1 (1980).
[2] M. E. Glicksman, M. B. Koss, and E. A. Winsa, Phys. Rev. Lett. **73**, 573 (1994).
[3] J. C. LaCombe, M. B. Koss, L. A. Tennenhouse, E. A. Winsa, and M. E. Glicksman, J. Cryst. Growth **194**, 143 (1998).
[4] T. Sawada, K. Takemura, K. Shigematsu, S. Yoda, and K. Kaawasaki, J. Cryst. Growth **158**, 328 (1996).
[5] T. Börzsönyi, T. Tóth-Katona, A. Buka, and L. Gránásy, Phys. Rev. Lett. **83**, 2853 (1999).
[6] T. Börzsönyi, T. Tóth-Katona, A. Buka, and L. Gránásy, Phys. Rev. E **62**, 7817 (2000).
[7] F. Banhart, E. Hernandez, and M. Terrones, Phys. Rev. Lett. **90**, 185502 (2003).
[8] M. Conti, in *Interface and Transport Dynamics*, edited by H. Emmerich, B. Nestler, and M. Schreckenberg, Lecture Notes in Computational Science and Engineering Vol.32 (Springer-Verlag, Berlin, 2003)
[9] M. Conti, Phys. Rev. E **64**, 051601 (2001).
[10] G. Caginalp and J. Jones, Appl. Math. Lett. **4**, 97 (1991).
[11] D. W. Oxtoby and P. R. Harrowell, J. Chem. Phys. **96**, 3834 (1992).
[12] D. M. Anderson, G. B. McFadden, and A. A. Wheeler, Physica D **135**, 175 (2000).
[13] X. Tong, C. Beckermann, and A. Karma, Phys. Rev. E **61**, R49 (2000).
[14] W. W. Mullins and R. F. Sekerka, J. Appl. Phys. **35**, 444 (1964).
[15] G. P. Ivantsov, Dokl. Akad. Nauk SSSR **58**, 56 (1947).
[16] M. Conti, F. Marinozzi, and U. Marini Bettolo Marconi, Phys. Rev. E **55**, 3087 (1997).